Available online at www.sciencedirect.com
ScienceDirect
Journal of Molecular Catalysis A: Chemical 273 (2007) 265–276
JOURNAL OF MOLECULAR CATALYSIS A: CHEMICAL
www.elsevier.com/locate/molcata

Catalytic properties of bimetallic NiCoB nanoalloy catalysts for hydrogenation of *p*-chloronitrobenzene

Jia-Huei Shen, Yu-Wen Chen *

Department of Chemical Engineering, Nanocatalysis Research Center, National Central University, Chung-Li 320, Taiwan, ROC

Received 1 December 2006; received in revised form 9 April 2007; accepted 15 April 2007
Available online 19 April 2007

Abstract

Nanosized NiCoB amorphous alloy catalysts with Co/Ni ratios varying from 0 to 3 were prepared by chemical reduction of nickel acetate and cobalt acetate with sodium borohydride in methanolic solution at room temperature under N_2 gas with vigorous stirring. The catalysts were characterized by nitrogen sorption, X-ray diffraction (XRD), transmission electron microscopy (TEM), differential scanning calorimetry (DSC), and X-ray photoelectron spectroscopy (XPS). NiCoB catalysts were tested for liquid-phase hydrogenation of *p*-chloronitrobenzene (*p*-CNB). The liquid-phase hydrogenation of *p*-CNB was carried out at 1.2 MPa hydrogen pressure, 373 K reaction temperature, methanol as reaction medium, 500 rpm stirring speed, 0.2 M *p*-CNB and 2 mmol Ni catalysts. The molar ratios of Co/Ni in the starting materials affected the concentrations of boron bounded to the nickel and cobalt metals, resulting in the change of surface area, electronic structures of the metals and catalytic activities of the catalysts. Nickel is enriched on the surface. Doping Co in NiB decreased the particle size and increased the stability of the NiCoB amorphous alloys. Doping Co in NiB increased the boron content, which in turn increased the electron density of Ni. The sample NiCoB(1:0.1) (the value in the bracket is the Ni:Co ratio in bulk) had the highest surface area of 23.5 m^2/g and the smallest particle size. TEM micrographs show that Co can reduce the particle size of NiB catalyst. DSC patterns demonstrated that the addition of cobalt suppressed the growth of crystalline structure of NiB. Adding small amount of cobalt to the NiB catalyst increased the surface area and reaction activity, but decreased the selectivity for the desired product, *p*-chloroaniline (*p*-CAN). However, overdosed cobalt had an opposite effect on Ni catalyst, i.e., reduced the reaction activity and increased the selectivity for *p*-CAN. The Co-dopant could weaken the extent of electron donation from the Ni atoms to the aromatic ring in *p*-CAN, which would further suppress the hydrodechlorination of *p*-CAN. The selectivity for *p*-CAN was also a function of conversion of *p*-CNB. Based on the electron transfer between elemental nickel and boron, NiCoB(1:0.1) had the most d-band electrons and the highest activities in hydrogenation of nitro group and dechlorination. The results can be interpreted by the electronegativity of the functional groups.

Keywords: NiCoB amorphous alloy; Nanometal; Nickel boride; *p*-Chloronitrobenzene; Liquid-phase hydrogenation

1. Introduction

Hydrogenation of halo-nitroaromatics to the corresponding halo-anilines was at one time a formidable problem, which has now found satisfactory solutions practiced industrially on a large scale. Aromatic halo-amines are used extensively in industrial applications in the production of fine chemicals, i.e., dyes, herbicides, pesticides, etc. The main route for their production is the selective hydrogenation of the corresponding nitro compounds over heterogeneous metal catalysts. Dehalogenation has been found to occur with palladium [1–3], platinum [1–3], rhodium [4], nickel [5], and copper chromite [6] catalysts. Among these, palladium, platinum, and rhodium are noble metals, which limit their implementation to industrial applications because of cost-effectiveness.

Depending on the halogen and its position relative to the nitro group in the aromatic system, dehalogenation can vary from negligible to 100%. In order to achieve high yields of halo-anilines, many approaches have been developed either by controlled preparation of the catalysts (alloying [7], controlling the metal particle dispersion and metal–support interaction [8], etc.) or the use of specific additives (promoters or inhibitors) [9–11].

In the reaction of *p*-chloronitrobenzene (*p*-CNB), its nitro group may be hydrogenated or it may be dehalogenated (see Fig. 1). Yu and Liu [12] have reported the selective hydrogena-

* Corresponding author. Tel.: +886 3 4227151x34203; fax: +886 3 4252296.
E-mail address: ywchen@cc.ncu.edu.tw (Y.-W. Chen).

1381-1169/$ – see front matter © 2007 Published by Elsevier B.V.
doi:10.1016/j.molcata.2007.04.015

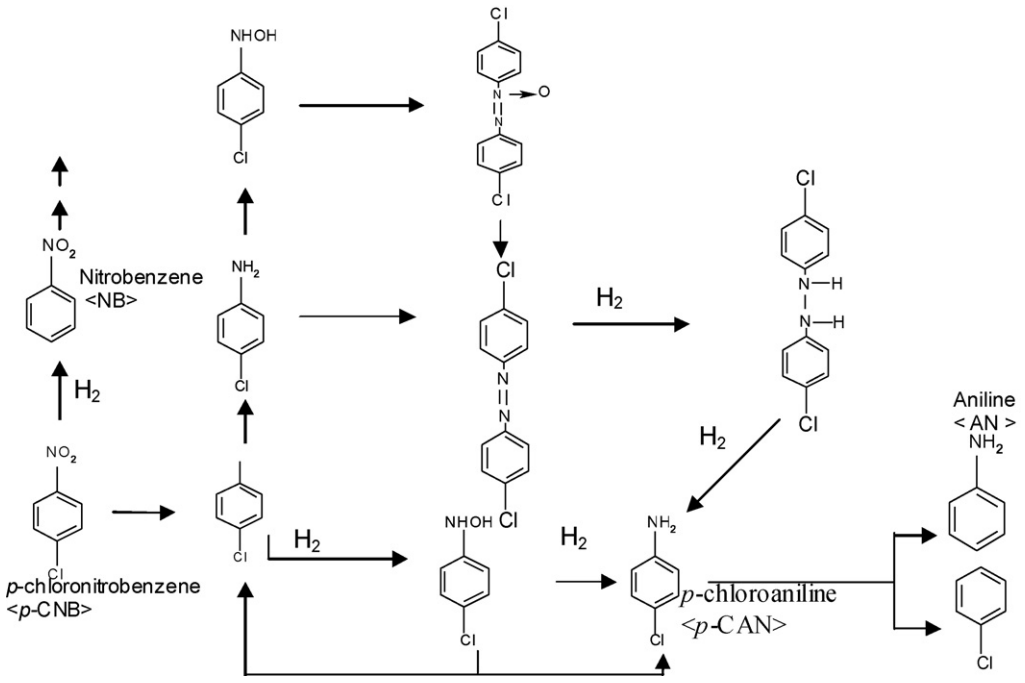

Fig. 1. Reaction scheme of hydrogenation of *p*-CNB.

tion of *o*-chloronitrobenzene to *o*-chloroaniline on Pt catalysts. Besides the desired product *o*-chloroaniline, many byproducts such as aniline, nitrobenzene, *o*-chlorophenylhydroxylamine, *o*-chloronitrosobenzene, azo- and azoxy-dichlorobenzenes, and chlorobenzene were formed at the same time.

Hydrogenation of *p*-CNB has been known to be an industrially important process. It is usually catalyzed by two classes of solids: noble metals, such as platinum, palladium, ruthenium, rhodium, and Raney nickel [13–15].

Nanoparticles exhibit unique and excellent properties from a fundamental and technological viewpoint. Recently, more and more researchers realized that ultrafine amorphous alloy particles could be new catalytic materials that exhibit attractive selectivity and activity for some reactions [16–19]. The nanocatalysts have more surface atoms and a higher concentration of highly coordinated unsaturated sites. Studies on ultrafine amorphous alloy particles have attracted much attention because of their interesting intrinsic properties, e.g., short-range order, long-range disorder, and high dispersion, as well as their potential applications, e.g., in powder metallurgy, magnetic materials, catalysts, and ferrofluids. The powder samples obtained by chemical reduction are highly dispersed and can be compacted to serve for different purposes. The ultrafine amorphous alloy powders combine the features of amorphous and ultrafine powder and have properties that are of interest in catalysis: (1) the presence of a large number of coordinatively unsaturated surface sites, (2) the lack of crystal defects, and (3) the isotropic, single phase nature of the materials. Nanosized Ni catalyst modified with boron has been reported to be a good catalyst for the hydrogenation of nitrobenzene and furfural [15,20–23]. In order to implement amorphous metal alloys as catalysts, some problems need to be solved. One problem among them is to find a method for increasing the surface area of the amorphous alloy and stabilizing the amorphous state during the reaction process. In other words, to produce smaller particles at nano scale and to enhance the thermal stability of catalysts are the focus of many researches on amorphous catalysts. The catalytic properties are highly dependent upon the preparation method [24,25]. Many systematic studies have been made on catalytic properties for NiB catalysts [26–33].

Bimetallic catalysts have been studied to discover the relationship between catalytic activity and the metal structure [34]. Many types of stable bimetallic particles have been reported, such as platinum–copper [35], platinum–rhodium [36], rhodium–gold [36], palladium–copper [37], palladium–gold [38], palladium–nickel [39], platinum–cobalt [40], etc. However, very few on NiCo catalysts have been reported [41–45]. Nitta et al. [41] investigated the formation of α, β-unsaturated alcohols from α, β-unsaturated aldehydes, finding that CoB catalysts has higher selectivity than NiB catalyst but that CoB catalyst has lower activity for the formation of olefins from acetylenes. The differences in the adsorption strength of reactants on Co and Ni metal resulted in the differences between the two catalysts. In 1997, Shen et al. [42] studied the structure of ultrafine NiCoB amorphous alloy by analysis of the extended X-ray absorption fine structure (EXAFS) spectra, and concluded that the catalytic activity of the ternary amorphous alloy NiCoB for the hydrogenation of benzene is related to both the nickel content and the structural disorder; the latter is mainly adjusted by the cobalt content. They also pointed out that cobalt acted as a chemical modifier and may have caused a structural change or electronic effect on the amorphous NiB. In the previous studies [25,46–49], the authors have reported the application of NiB catalysts in hydrogenation of *p*-CNB. They showed that the different preparation conditions affect the morphology, particle size, and surface area of the catalyst. The NiB catalyst

was passivated by boron; it was more stable than Raney nickel and did not catch fire after exposure to air. The NiB catalysts prepared at 298 K under a N_2 flow with vigorous stirring had smaller particle size and higher activity for the hydrogenation of *p*-CNB. It is also more active than the Raney nickel catalyst. The lanthanum-promoted NiB catalyst was more stable than NiB. The La-NiB catalyst had higher activity for the hydrogenation of *p*-CNB when compared with the unpromoted NiB and Raney nickel catalyst. The effect of a lanthanum promoter can be attributed to the electronic modification of nickel by lanthanum. NiPB catalysts also had higher activity than NiB for the hydrogenation of *p*-CNB, which indicated that the promoting effect of alloying boron and phosphorus on the hydrogenation activity was mainly attributed to its modification on the nature of the Ni active sites, which became more highly unsaturated at higher boron and phosphorus contents. In a parallel study, the authors have found that CoB is not active for this reaction. It is interesting to investigate the catalytic properties of bimetallic NiCoB catalysts in this reaction.

In this study, a series of nanosized NiCoB amorphous alloy catalysts with various Ni/Co ratios was prepared. The catalysts were characterized by nitrogen sorption, X-ray diffraction (XRD), transmission electron microscopy (TEM), differential scanning calorimetry (DSC), and X-ray photoelectron spectroscopy (XPS). The catalysts were tested for liquid-phase hydrogenation of *p*-CNB.

2. Experimental

2.1. Materials

p-CNB, with a purity of >99%, was obtained from Acros (Belgium). High-purity hydrogen gas (>99.99% from Air Product) was used without further purification. Nickel acetate tetrahydrate (>98%) and cobalt acetate tetrahydrate (>98%) were supplied by Showa Chemicals (Tokyo, Japan). Sodium borohydride (>99%) was purchased from Lancaster (Morecambe, UK) and methanol (>99.9%) was from Tedia Co. (Ohio, USA). Double distilled water was used for the catalyst preparation.

2.2. Catalyst preparation

Nanosized NiCoB amorphous alloy catalysts were prepared by the chemical reduction of nickel acetate and cobalt acetate by borohydride in the solution at room temperature. A series of NiCoB catalysts with various compositions was prepared by mixing absolute methanol in deionized water solution of nickel acetate (20 ml, 0.1 M) and cobalt acetate at 298 K under vigorous stirring. The solution of sodium borohydride (6 ml, 1 M) was then added dropwise with a micro tubing pump into the mixture under a nitrogen stream. Excess amount of borohydride was used in order to completely reduce nickel and cobalt cations to metals. Various Ni/Co ratios in the starting materials were used in this study. The catalyst was denoted by NiCoB(*x*:*y*) where *x* and *y* are the atomic ratios of Ni and Co, respectively, in the starting materials.

2.3. Catalyst characterization

BET surface area was measured by nitrogen volumetric adsorption (Micromeritics ASAP 2010) at −196 °C. The temperature of the liquid nitrogen bath was checked by a thermistor probe. XRD measurements were recorded using a Siemens D500 powder diffractometer with CuKα radiation (40 kV, 30 mA). The sample was scanned over the range of $2\theta = 5$–60° to identify the amorphous structure. The morphology of the samples was determined by TEM performed on a JEOL JEM-1200 EX II electron microscope operating at 160 kV. Differential scanning calorimetry measurement was conducted under a nitrogen (99.99%) atmosphere on a Perkin-Elmer DSC instrument. The DSC experiment was carried out on samples in the temperature range of 50–560 °C at a rate of 10 °C/min. After etching the surface by Ar^+ ions for 15 min, the XPS spectra were recorded with a Thermo VG Scientific Sigma Probe spectrometer using Al Kα radiation (20 kV and 30 mA). The base pressure in the analyzing chamber was maintained in the order of 10^{-9} Torr. The spectrometer was operated at 23.5 eV pass energy. The catalyst sample was mounted quickly onto a grid attached to a sample holder, keeping the powder soaked in 99% ethanol to minimize the oxidation of the powder by air. After evacuating ethanol, the sample was transferred to the analyzing chamber. All the binding energy (BE) values were calibrated by using $C_{1s} = 284.6$ eV as a reference. The surface composition was determined by using 0.13, 2.43, and 2.5 as the PHI sensitivity factors to B_{1s}, $Ni_{2p3/2}$, $Co_{2p3/2}$, respectively.

2.4. Catalytic activity

All the experiments were carried out in a cylindrical stirred-tank reactor (Parr Instrument Model 4842) with a capacity of 160 ml. A four-bladed pitched impeller was placed for effective agitation, and the agitator was connected to an electric motor. A pressure transmitter and an automatic temperature controller were also provided. The gases were supplied from cylinders and introduced into the bottom of the reactor; a separate tube was served as a sampling tube for the liquid phase.

The activity of the catalysts was tested for the selective hydrogenation of *p*-CNB. The reactor was filled with 2 mmol Ni catalyst, and 2.52 g *p*-CNB in 80 ml absolute methanol solution, which serves as the reaction medium. Previous finding [50] proved that methanol is a better reaction medium than ethanol. Air was flushed out of the reactor by passing hydrogen at room temperature and hydrogen was then fed into the reactor. During the run, samples were withdrawn periodically (10 min) and analyzed by a gas chromatograph equipped with flame ionization detector and a 3 m × 1/8 in. stainless-steel column packed with 5% OV-101 on Chromsorb WAW-DMSC (80–100 mesh). It has been confirmed that the reaction was carried out under a kinetically controlled regime.

The conversion and selectivity to product were calculated as follows:

$$\text{Conversion}\,(\%) = \left(1 - \frac{C_{p\text{-CNB}}}{C_{\text{AN}} + C_{\text{NB}} + C_{p\text{-CAN}} + C_{p\text{-CNB}}}\right) \times 100$$

$$S_{AN}(\%) = \left(\frac{C_{AN}}{C_{AN} + C_{NB} + C_{p\text{-CAN}}}\right) \times 100$$

$$S_{NB}(\%) = \left(\frac{C_{NB}}{C_{AN} + C_{NB} + C_{p\text{-CAN}}}\right) \times 100$$

$$S_{p\text{-CAN}}(\%) = \left(\frac{C_{p\text{-CAN}}}{C_{AN} + C_{NB} + C_{p\text{-CAN}}}\right) \times 100$$

where C_{AN}, C_{NB}, $C_{p\text{-CAN}}$, and $C_{p\text{-CNB}}$ represent the concentrations of aniline, nitrobenzene, *p*-chloroaniline (*p*-CAN), and *p*-CNB, respectively. The reproducibility of the results was checked by repeating the runs at least three times on the same batch of the catalyst and another two times for a different batch of the catalyst; the experimental error was found to be within 5%.

3. Results and discussion

3.1. Catalyst characterization

Table 1 lists the composition, surface area, and atomic ratio of the catalysts. The composition on the surface of the samples was determined by XPS. From the atomic ratio, it can be observed that the precipitating capacity of boron increased with an increase in the cobalt content. Comparison of the atomic ratios of NiB ($NiB_{0.175}$) with those of CoB ($CoB_{0.89}$), clearly shows that cobalt can hold more boron than nickel. Therefore, addition of cobalt facilitates the precipitation of boron in the catalysts. It should be noted that boron can donate partial electrons to metal. Therefore, it is favorable to have higher boron contents in the catalyst. Since nickel and cobalt were reduced immediately by the addition of $NaBH_4$, the ratios of Ni/Co in bulk of the catalysts should be exactly the same as those in the starting materials. It is also shown in Table 1 that the Ni/Co ratio on surface is higher than that in bulk, indicating the surface is enriched with Ni.

The surface area of the samples was determined by BET analysis. The composition of the starting materials significantly influenced the morphology and particle size of the NiCoB amorphous catalysts, subsequently affecting the surface area of the catalysts. The sample NiCoB(1:0.1) had the largest surface area (23.5 m^2/g). The surface area decreased in the following order: NiCoB(1:0.1) (23.5 m^2/g) > NiB (23.1 m^2/g) > NiCoB(1:0.3) (21.5 m^2/g) > NiCoB(1:3) (17.9 m^2/g) > NiCoB (1:1) (17.0 m^2/g) > CoB (16.9 m^2/g). However, the differences are not significant. The particle sizes of all the samples are in the nanosize range. Nevertheless, the BET surface area of NiCoB decreased with an increase in the cobalt content in the sample. Since the catalysts were treated at 120 °C before nitrogen sorption measurements, which would cause aggregation and/or sintering of metal to some extent, the data from BET might not be the exact values for as-prepared samples and they could be underestimated. Nevertheless, they showed that the samples were still in the nanosize range even at 120 °C.

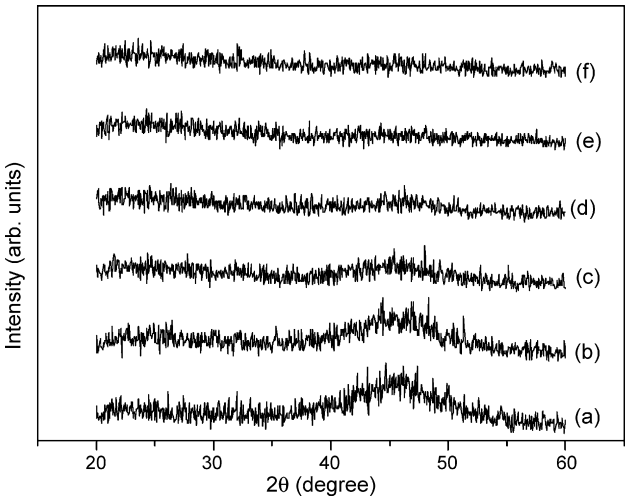

Fig. 2. XRD patterns of the samples: (a) NiB, (b) NiCoB(1:0.1), (c) NiCoB(1:0.3), (d) NiCoB(1:1), (e) NiCoB(1:3), and (f) CoB.

For NiB catalysts, the specific amorphous structure was a key point for the reason that they owned several interesting intrinsic properties, such as short-range order, long-range disorder, the presence of a large number of coordinatively unsaturated surface sites and the lack of crystal defects and isotropic, single phase nature of the materials. In other words, this amorphous structure was beneficial for hydrogenation reactions. The objective of the introduction of second metal was to promote the catalytic activity and the thermal resistance of catalyst particles. After promotion, however, to maintain the special structure or to enhance the thermal stability was an important consideration for the catalytic modification. The XRD patterns of NiB, CoB, and NiCoB samples with various contents of Co are illustrated in Fig. 2. A single broad peak around $2\theta = 45°$ in each pattern indicates the amorphous phase of all the as-prepared samples, in consistent with those in literature [33,51]. Notably, the patterns contained no distinct peak corresponding to a crystalline phase of nickel, cobalt, or boron. XRD mainly detects particles larger than 4 nm; the smaller the peak intensity, the smaller is the crystallite size. The results show that the particle size of

Table 1
Physicochemical properties of the NiB, CoB, and NiCoB catalysts

Catalyst	Surface composition	Atomic ratio	Ni/B (atomic ratio)	Ni/(Co + B) (atomic ratio)	Surface area (m^2/g)
NiB	$Ni_{85.09}B_{14.92}$	$NiB_{0.175}$	5.703	5.703	23.1
NiCoB(1:0.1)	$Ni_{67.88}Co_{4.1}B_{28.57}$	$NiCo_{0.06}B_{0.42}$	2.376	2.078	23.5
NiCoB(1:0.3)	$Ni_{50.43}Co_{14.98}B_{34.59}$	$NiCo_{0.30}B_{0.68}$	1.458	1.017	21.5
NiCoB(1:1)	$Ni_{35.59}Co_{31.22}B_{33.20}$	$NiCo_{1.14}B_{0.93}$	1.072	0.552	17.0
NiCoB(1:3)	$Ni_{19.59}Co_{36.16}B_{44.25}$	$NiCo_{1.84}B_{2.26}$	0.443	0.243	17.9
CoB	$Co_{52.89}B_{47.11}$	$CoB_{0.891}$	0	0	16.9

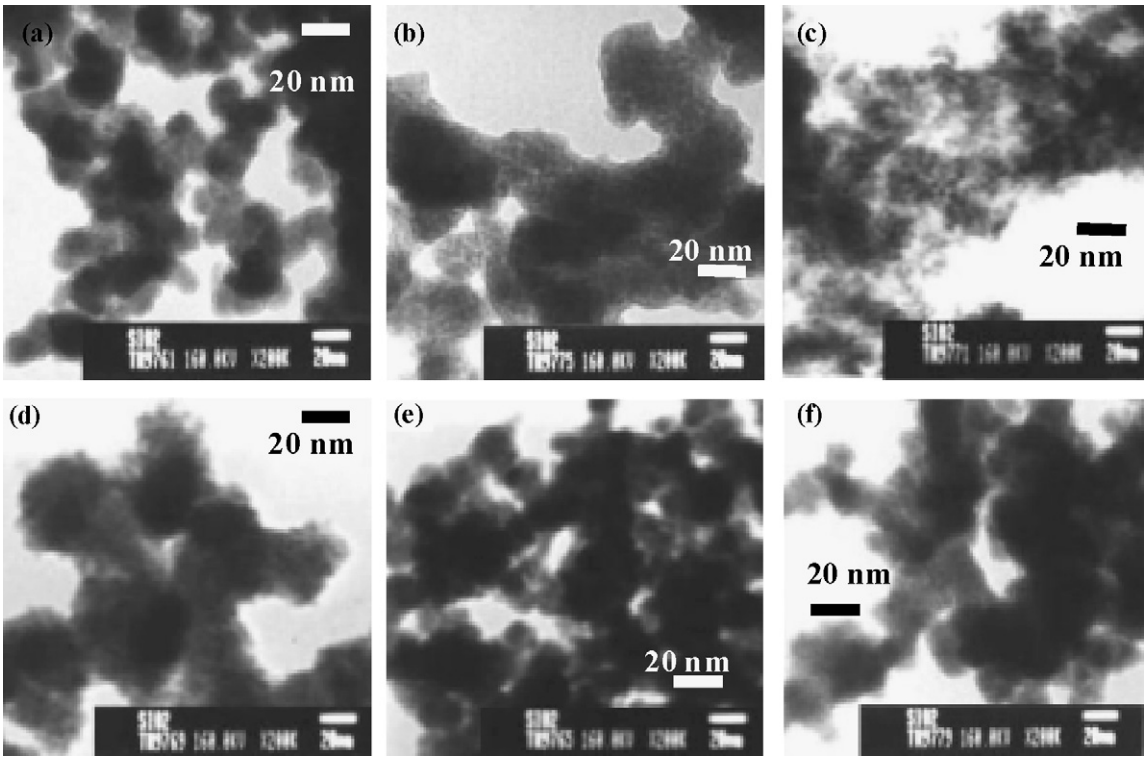

Fig. 3. TEM pictures of the samples: (a) NiB, (b) NiCoB(1:0.1), (c) NiCoB(1:0.3), (d) NiCoB(1:1), (e)NiCoB(1:3), and (f) CoB.

all the as-prepared samples was less than 4 nm. In addition, the peak intensity decreased with an increase in the cobalt content, indicating that the addition of cobalt into the NiB catalyst can reduce the particle size.

The morphology of NiCoB samples was determined by TEM as shown in Fig. 3. Each sample comprised of uniformly spherical particles and existed as nanometer particles. NiCoB had smaller particles than NiB. The particle size of NiCoB(1:0.1) in Fig. 3 is about 4–5 nm, but the sample may be formed by self-aggregation of some particles due to the extremely high specific surface energy of the nanometer particle [52]. This result is in agreement with that of XRD results. Yu et al. [44] observed some gel-like clusters in the NiCoB samples and the amount of the clusters increased with an increase in the cobalt content because cobalt ion readily forms hydroxide easier than nickel ion. It should be noted that their samples were prepared in aqueous solution by using KBH_4 as the reducing agent. In contrast, our samples were prepared in alcoholic solution by using $NaBH_4$. It is known that the sample prepared in alcoholic solution had smaller particle size. KBH_4 is a very strong reducing agent. The reduction rate would be too high and caused metal aggregation. Li et al. [62] reported the particle size around 20 nm. They also prepared the NiCoB samples in aqueous solution using KBH_4.

The crystallization behavior of NiCoB was analyzed by DSC. As shown in Fig. 4, the DSC profile changed significantly with the content of cobalt. There were two endothermal peaks at 325 and 475 °C for NiB. NiCoB(1:0.1) also had these two peaks, but the areas of these two peaks were smaller. NiCoB(1:0.3) not only had a smaller peak area, but also showed higher crystallization temperature. Adding cobalt into NiB catalysts could reduce the area of the endothermal peak and gradually make the crystallization temperature rise, indicating that cobalt could suppress the growth of the crystalline structure of NiB and help the NiB catalyst to maintain its amorphous state. Li et al. [62] have reported that Ni and Co in the NiCoB sample were present in the whole amorphous alloy rather than in the individual NiB and CoB amorphous alloys. The alloying of Ni and Co resulted in the shift of crystallization temperature towards that of the CoB amorphous alloy. Our results are in accord with literature reports.

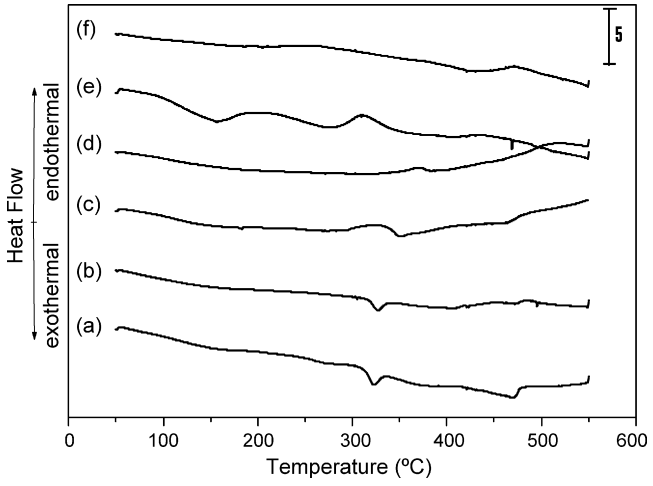

Fig. 4. DSC profiles of the samples: (a) NiB, (b) NiCoB(1:0.1), (c) NiCoB(1:0.3), (d) NiCoB(1:1), (e) NiCoB(1:3), and (f) CoB.

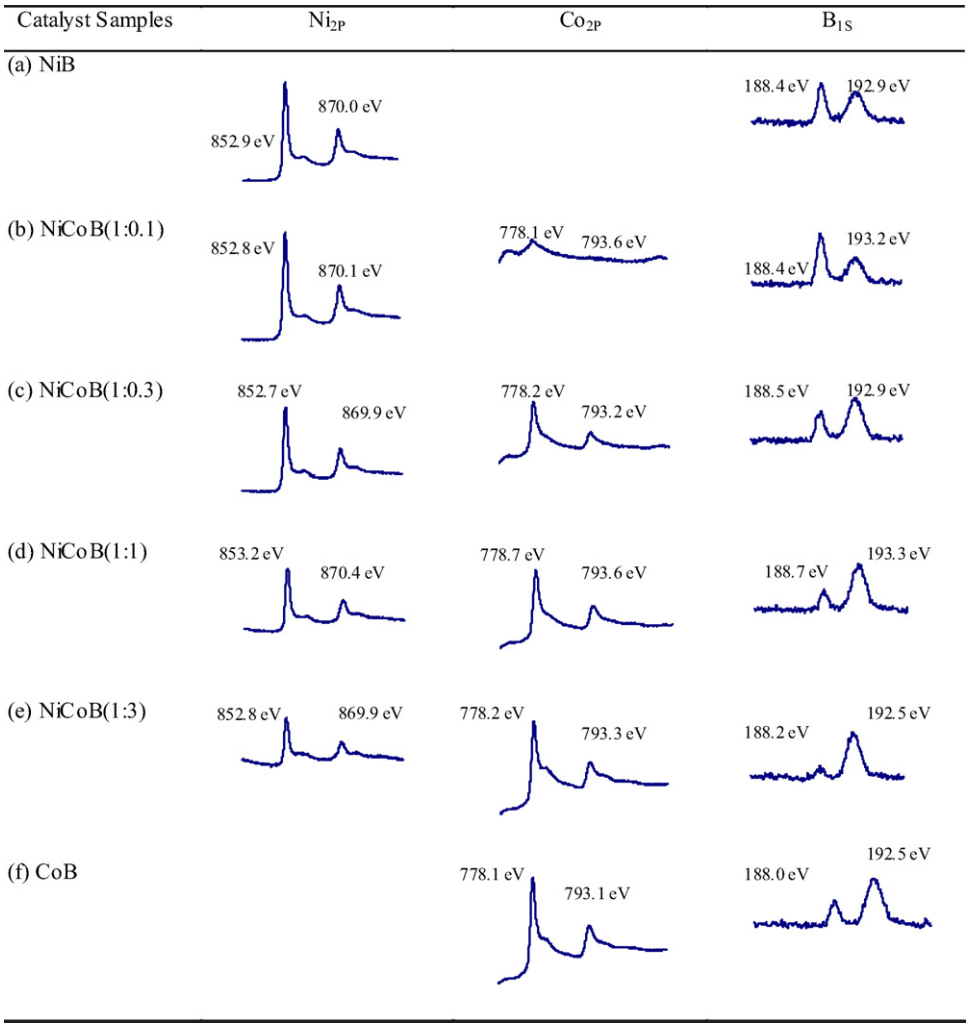

Fig. 5. XPS spectra of the samples: (a) NiB, (b) NiCoB(1:0.1), (c) NiCoB(1:0.3), (d) NiCoB(1:1), (e) NiCoB(1:3), and (f) CoB.

Yu et al. [44] reported that the DSC patterns of NiCoB samples were quite similar to those of corresponding mixed NiB and CoB, when $X_{Co} < 10\%$. When $X_{Co} > 10\%$, the DSC patterns of NiCoB were different from either of the pure NiB and CoB or the mixture of NiB and CoB. In contrast, our results showed that adding even a small amount of Co into NiB changes the structure significantly. The capacity of cobalt in the sample NiCoB(1:0.1) was found to be 10% and its DSC patterns resemble the mixture of the patterns of NiB and CoB. But the patterns of NiCoB(1:0.3) and NiCoB(1:1) were also similar to the pattern of NiCoB(1:0.1); just with the increase in the content of cobalt, the area of endothermal peaks gradually decreased and the crystallization temperatures rose gradually.

The XPS spectra of NiCoB powders are shown in Fig. 5. The binding energy of all samples did not shift obviously with increasing cobalt loading. The surface composition could be further determined by the analysis of relative peak areas in the XPS spectra. An example of peak deconvolution of NiCoB(1:1) is shown in Fig. 6. Fig. 6a shows $Ni_{2p2/3}$ level, in which five Lorentzian–Gaussian peaks were separated to reveal the behavior of the satellite peaks. The peak at 852.7 eV is attributed to

Table 2
Relative peak areas in the XPS spectra

Catalyst	Surface composition (atomic ratio)	$Ni_{2p3/2}$		$Co_{2p3/2}$		B_{1s}	
		Ni^0	Ni^{2+}	Co^0	Co^{2+}	B^0	B^{3+}
NiB	$Ni_{85.09}B_{14.92}$	63.2%	15.0%			37.7%	62.3%
NiCoB(1:0.1)	$Ni_{67.88}Co_{4.1}B_{28.57}$	63.2%	14.2%	46.6%	33.0%	51.3%	48.7%
NiCoB(1:0.3)	$Ni_{50.43}Co_{14.98}B_{34.59}$	68.3%	7.1%	51.9%	28.3%	30.0%	70.0%
NiCoB(1:1)	$Ni_{35.59}Co_{31.22}B_{33.20}$	50.4%	24.4%	48.1%	27.6%	19.0%	81.0%
NiCoB(1:3)	$Ni_{19.59}Co_{36.16}B_{44.25}$	60.0%	10.6%	44.4%	30.2%	10.8%	89.2%
CoB	$Co_{52.89}B_{47.11}$			45.7%	30.3%	23.1%	76.9%

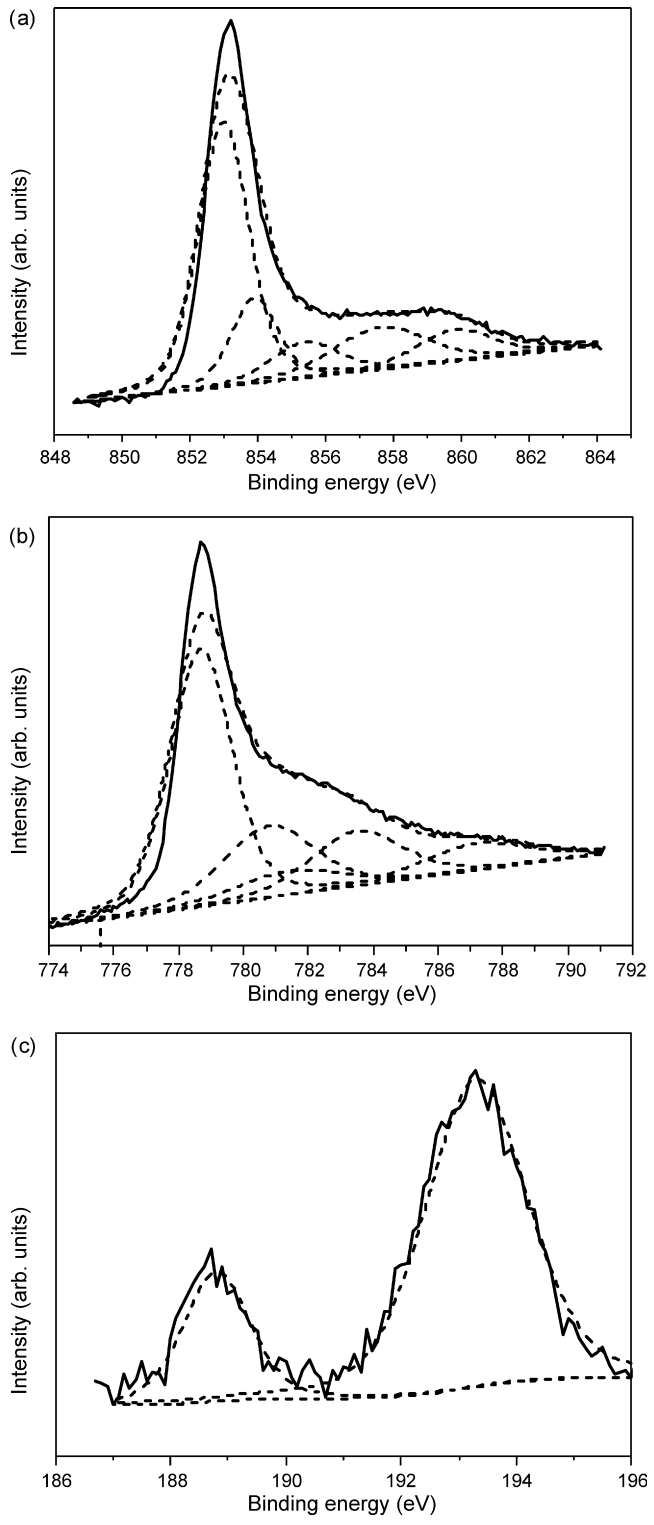

Fig. 6. Peak deconvolution of: (a) $Ni_{2p3/2}$, (b) $Co_{2p3/2}$, and (c) B_{1s} level for amorphous NiCoB alloy powder.

the elemental nickel [53]. The presence of NiO and $Ni(OH)_2$ are confirmed by fitting the high energy shoulders on the metallic Ni line at about 853.8 and 855.6 eV (Table 2) [45,53,54]. The peaks at 856.8 and 858.7 eV are ascribed to the NiO multiple splitting peaks and the Ni electron energy-loss peak [45,55]. Since only the areas of two peaks were referred to Ni^{2+}, the other two peaks were not included in calculations; the sum of the peak areas of Ni^0 and Ni^{2+} are not 100%. The deconvolution of $Co_{2p3/2}$ spectrum is shown in Fig. 6b, which is similarly separated to five Lorentzian–Gaussian peaks; elemental state is at 778.3 eV [53], CoO and $Co(OH)_2$ being present at 780.4 and 781.0 eV [53,56]. The peaks at 783.1 and 786.8 eV are ascribed to the electron shakeup peak of $Co(OH)_2$ and CoO multiple splitting peaks [56]. The peaks of B_{1s} at 188.7 and 193.7 eV are corresponding to the elemental boron and oxidized boron, respectively [45,57,58], and the separated spectrum is shown in Fig. 6c. In comparison with the binding energy of the pure boron (187.1 eV), the binding energy of elemental boron in NiB or NiCoB positively shifts by about 1.6 eV, indicating that the boron donates partial electron to the alloying nickel. The electron transfer makes B electron-deficient and Ni metal electron-enriched. Li et al. [62] reported that the metallic Ni accepted more electrons from the alloying B than the metallic Co in the NiCoB amorphous alloys. The higher electron density of Ni atom in the NiCoB catalyst was mainly attributed to the B-enrichment. The increase in the B content would contribute more electrons to the metallic Ni.

Table 2 illustrates the relative peak areas in the XPS spectra. In the sample NiB, the content of elemental nickel is four times the content of oxidized nickel. In the sample CoB, the content of elemental cobalt is two times the content of oxidized cobalt. The results show that cobalt is easier to be oxidized than nickel in metal-boron catalysts. It is also shown that adding a small amount of Co into NiB can reduce the formation of nickel oxides. However, the content of elemental nickel decreased in NiCoB(1:3) due to higher Co loading. Although the content of elemental nickel in NiCoB(1:3) is still quite high (60%), the surface composition of Ni is only 20 %, which is too low to show high activity.

By multiplying the peak areas of each species in the XPS spectra by the concentration of each element on the surface, the proportion of each species can be obtained as shown in Table 3. For example, the concentration of nickel in the sample NiCoB(1:0.1) ($Ni_{67.88}Co_{4.1}B_{28.57}$) is 68%, among which 63% is Ni^0 and 14% is Ni^{2+}, and then the composition of Ni^0 is 43% and that of Ni^{2+} is 10%.

There is a modest electron transfer between neighboring elemental nickel and elemental boron in the NiB catalyst as boron donates part of electrons to the alloying nickel. Since the oxidized state is very stable, the electron transfer only occurs between elemental nickel and elemental boron. For the activation of the N–O bond, more electron transfer in nickel metal facilitates the catalyst to attract the partial negative oxygen easily, and hydrogen can also attack the partial positive nitrogen easily, whereby the completion of reaction gets accelerated. The higher the content of elemental nickel and boron is, the more the electron transfer is, and the faster is the reaction. Although the content of elemental nickel in NiB (54%) is high, the boron content is too low for electron transfer. NiCoB(1:0.1) has the highest activity, because it has high concentration of elemental nickel (43%) and elemental boron (15%). The electron density of nickel is increased by the electron donation from boron to nickel [59].

Table 3
Compositions of various species in the catalysts

Catalyst	Surface composition (atomic ratio)	$Ni_{2p3/2}$		$Co_{2p3/2}$		B_{1s}	
		Ni	Ni^{2+}	Co	Co^{2+}	B	B^{3+}
NiB	$Ni_{85.09}B_{14.92}$	0.54	0.13			0.06	0.09
NiCoB(1:0.1)	$Ni_{67.88}Co_{4.1}B_{28.57}$	0.43	0.10	0.02	0.01	0.15	0.14
NiCoB(1:0.3)	$Ni_{50.43}Co_{14.98}B_{34.59}$	0.34	0.04	0.08	0.04	0.11	0.24
NiCoB(1:1)	$Ni_{35.59}Co_{31.22}B_{33.20}$	0.18	0.24	0.15	0.09	0.06	0.27
NiCoB(1:3)	$Ni_{19.59}Co_{36.16}B_{44.25}$	0.12	0.02	0.16	0.11	0.05	0.40
CoB	$Co_{52.89}B_{47.11}$			0.24	0.16	0.11	0.36

3.2. Catalytic activity

The catalytic activity of the as-prepared catalysts was tested for the hydrogenation of *p*-CNB. In this study, *p*-CAN is the primary product for all NiB and NiCoB catalysts. CoB did not show any activity in this reaction condition. Fig. 7 shows the time–conversion curves of *p*-CNB for NiB and NiCoB catalysts. It shows that the reaction follows first order with respect to *p*-CNB. The sample NiCoB(1:0.1) had the highest reaction rate, its conversion of *p*-CNB reaching 70% within 20 min at 373 K, and 100% within 40 min. Table 4 shows the effect of cobalt content on the hydrogenation of *p*-CNB over NiB and NiCoB catalysts. While NiCoB(1:0.1) showed the highest reaction rate, its selectivity to *p*-CAN is low. The selectivity to *p*-CAN was 95.1% when the conversion of *p*-CNB achieved 73.8% at 20 min over NiCoB(1:0.1). The selectivity to *p*-CAN over NiCoB(1:0.3) was only 92.5% at 30 min when the conversion of *p*-CNB was 85.2%. NiB gave 83.2% conversion of *p*-CNB within 50 min, and the selectivity to *p*-CAN was 98.9%. The selectivity to *p*-CAN over NiCoB(1:1) was 97.0% at 80 min, when the conversion of *p*-CNB was 91.3%. NiCoB(1:3) exhibited the lowest reaction rate; it achieved 100% conversion of *p*-CNB at 170 min, but had a higher selectivity to *p*-CAN (96.2%). Since *p*-CAN is the intermediate product in a series of reaction, it is expected that the selectivity to *p*-CAN is lower if the catalyst is too active. The NiCoB amorphous alloy catalyst could be reused more than five times, whereas NiB lost 30% activity after used three times.

Fig. 8 shows the compositions of the reaction solution for the maximum selectivity to *p*-CAN for each catalyst. It clearly shows that the selectivity to *p*-CAN decreased in the following order: NiCoB(1:3) > NiCoB(1:1) > NiB > NiCoB(1:0.1) > NiCoB(1:0.3). In general, it is in the reverse order of activity, as expected.

Fig. 9a shows the activity with respect to $Ni^0/(Ni^0 + Co^0)$. The activity increased with an increase in $Ni^0/(Ni^0 + Co^0)$ for all NiCoB samples. This confirms that metallic nickel is the active site for hydrogenation reaction. As shown in Fig. 9b, the activity also increased with an increase in $B^0/(B^0 + B^{3+})$ for all NiCoB samples, indicating that boride (B^0) can donate partial electrons to Ni^0 and enhance the reaction. The more B^0 around Ni^0 is, the higher are the activity and reaction rate. When NiB is compared with NiCoB(1:1), both samples had the same contents of elemental boron (6%), but the content of elemental nickel in NiB (54%) was about three times of that in NiCoB(1:1:3) (18%). This proves the enhanced activity of NiB in the hydrogenation of *p*-CNB to *p*-CAN than that of NiCoB(1:1).

Fig. 10 shows the activity of NiB and NiCoB catalysts for the hydrogenation of *p*-CNB. Fig. 11 shows the simplified reaction scheme for the hydrogenation of *p*-CNB. Hydrogenation of *p*-CNB follows two paths in the beginning of reaction, one

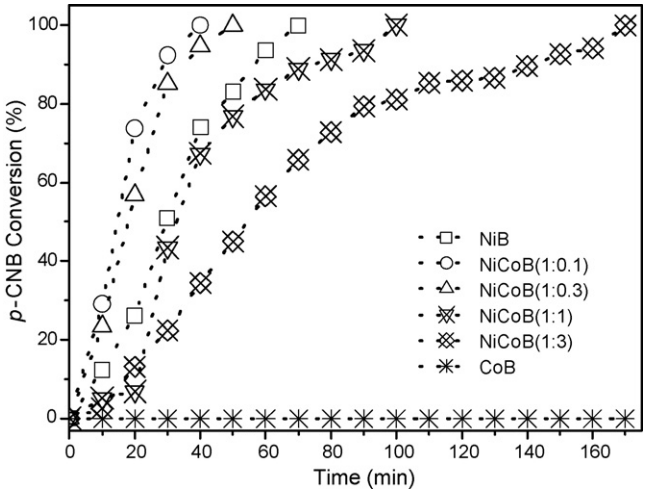

Fig. 7. Time–conversion curves of *p*-CNB hydrogenation on NiB and NiCoB catalysts (reaction condition: 373 K, 1.2 MPa, 500 rpm, 0.2 M *p*-CNB and 2 mmol Ni catalysts).

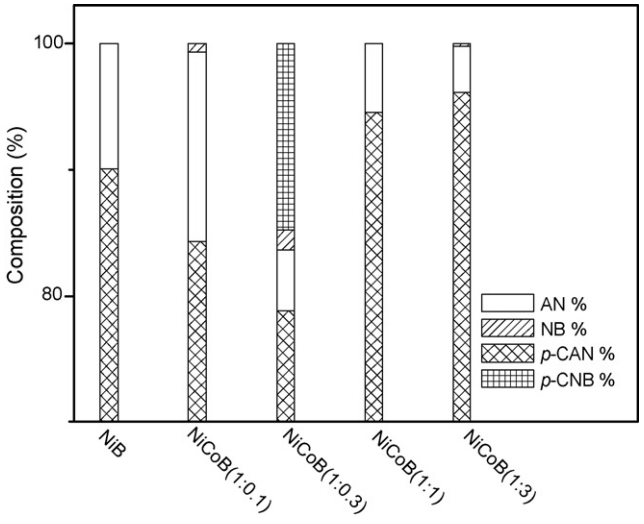

Fig. 8. Effect of cobalt content on the hydrogenation of *p*-CNB over NiB and NiCoB catalysts.

Table 4
Hydrogenation of *p*-CNB over NiB and NiCoB catalysts

Sample	Reaction time (min)[a]	*p*-CNB conversion[a] (%)	Selectivity[b] (%)		
			AN	NB	*p*-CAN
NiB	50	83.17	0.68	0.40	98.92
NiCoB(1:0.1:3)	20	73.75	1.06	3.89	95.06
NiCoB(1:0.3:3)	30	85.22	5.63	1.88	92.49
NiCoB(1:1:3)	80	91.27	2.39	0.60	97.01
NiCoB(1:3:3)	170	100	3.63	0.22	96.15

Reaction condition: 1.2 MPa hydrogen pressure, 373 K reaction temperature, absolute methanol medium, 500 rpm stirring speed, 0.2 M *p*-CNB and 2 mmol Ni catalyst.

[a] Time at which selectivity of *p*-CAN reached the maximum.

[b] AN: Aniline; NB: nitrobenzene; *p*-CAN: *p*-chloroaniline.

leading to the formation of nitrobenzene and the other to *p*-CAN. In either event, nitrobenzene, *p*-CAN, or aniline is the final product. Fig. 10 shows that in every case the concentration of nitrobenzene increased in 10 min, then decreased and completely converted to aniline. There are two possible explanations; one is that *p*-CNB reaction followed path (1) only in the beginning and not after 10 min, and the other is that the hydrogenation followed path (3), which is much faster than the rate following path (1). Since the increased range of aniline produced is not obvious, the possibility of latter is negligible.

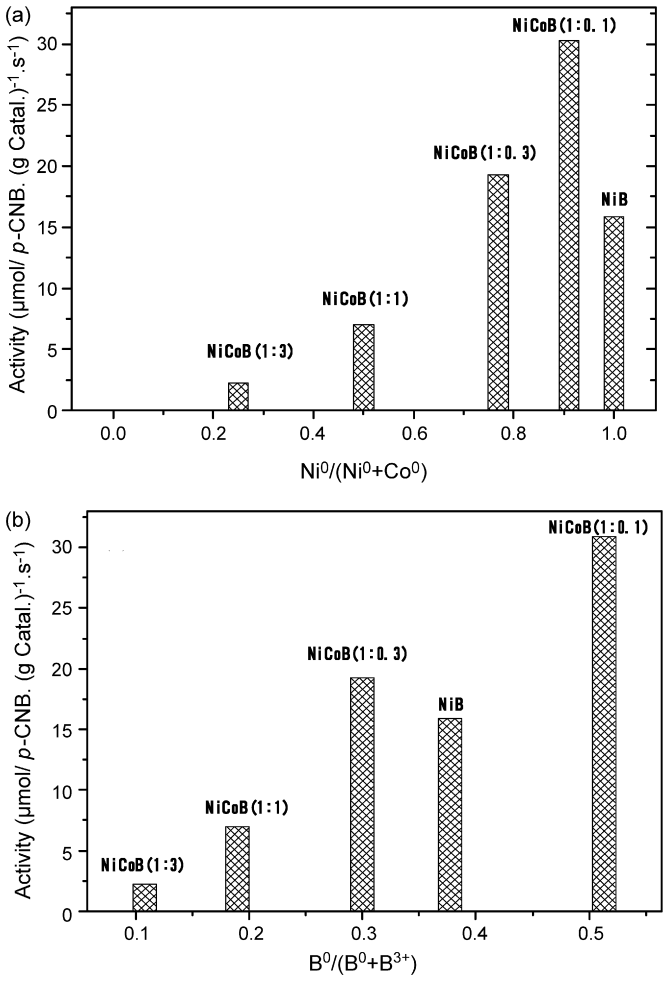

Fig. 9. Initial activities of NiB and NiCoB catalysts in hydrogenation of *p*-CNB. (a) $Ni^0/(Ni^0 + Co^0)$ vs. activity, (b) $B^0/(B^0 + B^{3+})$ vs. activity.

Fig. 12 shows the conversion–selectivity curve for NiB and NiCoB catalysts. The selectivity to *p*-CAN increased with an increase in conversion and then decreased, as expected. For NiCoB(1:1) and NiCoB(1:3) catalysts, the selectivity to *p*-CAN did not decrease after reaching the maximum, it was leveled off. It demonstrated that the hydrogenation of *p*-CNB was inhibited due to the higher content of cobalt. In other words, path (4) is suppressed by the addition of cobalt.

p-CNB has stronger adsorption on Ni catalyst than hydrogen. CoB exhibited lower activity than NiB due to its affinity stronger towards *p*-CNB and weaker with respect to H_2. NiCoB was more active than either NiB or CoB, owing to the weaker adsorption of *p*-CNB and stronger adsorption of H_2 on it. However, high concentration of Co and B on surface would decrease the number of active sites on the surface and resulted in decreased activity.

If the adsorption strength of substrate on the catalyst is slightly weakened, the activity of hydrogenation can be increased significantly [60]. Based on the electron transfer between elemental nickel and boron aforementioned, NiCoB(1:0.1) had the most d-band electrons and the highest activity. The electron donation of boron in the boride catalysts is possibly unfavorable on the adsorption of *p*-CNB.

The nitro group consists of two highly electronegative elements, N and O. Oxygen atom is even more electronegative than the nitrogen atom; hence, the N–O bond is polarized. The partially positive charge of the nitrogen atom, combined with high electronegativity, makes the nitro group easily reducible. Electron-rich Ni easily adsorbs both $–NO_2$ and –Cl which are electronegative. The para-substituted nitro group has the high electronegativity resulting from the combination of both inductive and resonance effects. For chlorine, only the inductive effect is present. The relative strength of the electron-withdrawing properties of nitro group and chlorine are 0.78 and 0.23, respectively [61]. Since the $–NO_2$ group is more electronegative than –Cl, $–NO_2$ is supposed to occupy the active site on the Ni surface at the start of the reaction. The $–NO_2$ group adsorbed on the catalyst surface is hydrogenated to form *p*-CAN which is further desorbed. When –Cl pre-occupied the catalyst surface,

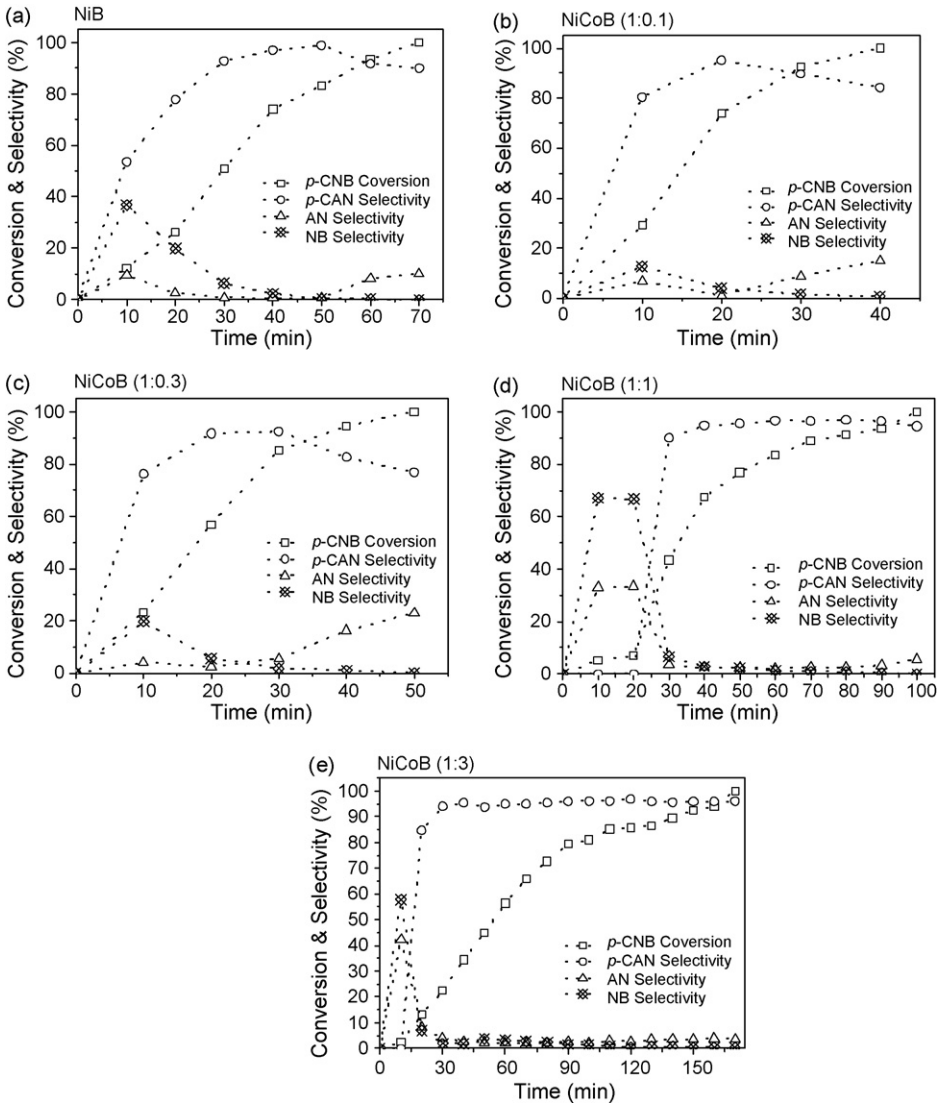

Fig. 10. Reaction activities of the hydrogenation of *p*-CNB to *p*-CAN catalyzed by ultrafine NiB and NiCoB amorphous alloy catalysts. (a) NiB, (b) NiCoB(1:0.1), (c) NiCoB(1:0.3), (d) NiCoB(1:1), and (e) NiCoB(1:3).

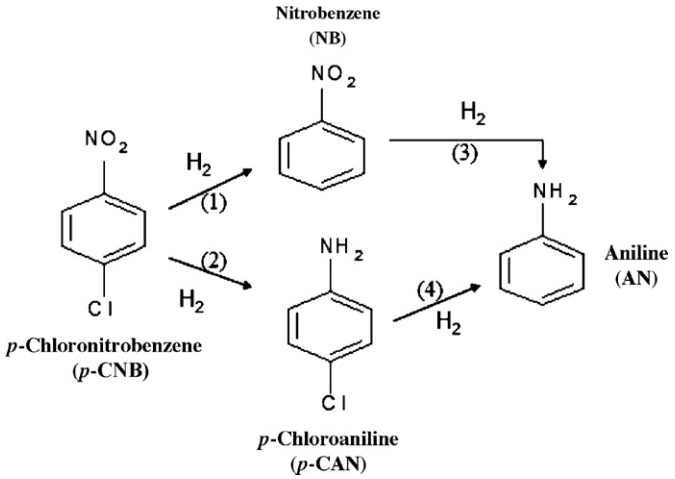

Fig. 11. Simplified reaction scheme of hydrogenation of *p*-CNB.

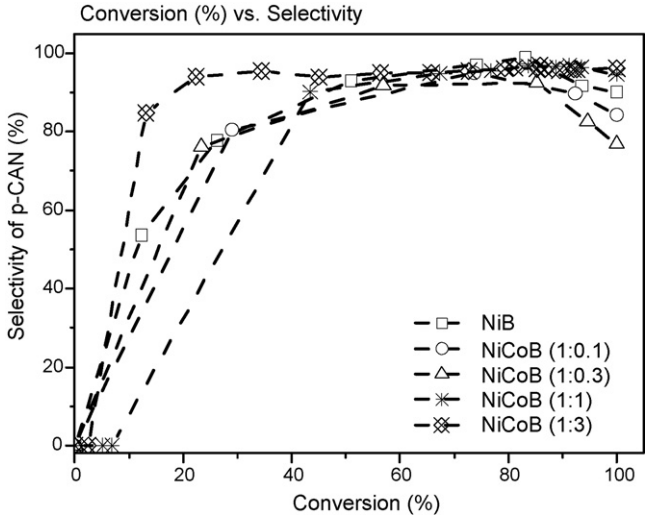

Fig. 12. *p*-CAN selectivity as a function of *p*-CNB conversion on NiB and NiCoB catalysts.

hydrogenation followed by dehalogenation occurred, leading to the formation of nitrobenzene which is eventually desorbed. It is possible that the desorbed nitrobenzene would re-adsorb on the catalyst surface. As a result of the chemical bonding in the nitro group, the nitrogen atom is positively charged and each oxygen atom has a partial negative charge. For this reason the nitro group strongly attracts electrons. Both $–NO_2$ and –Cl are electronegative, so they have the same tendency to adsorb on electron-rich nickel. Therefore, dehalogenation increases as the reaction proceeds. Since boron can donate electrons to nickel, the more electron transfer is, the more electron-rich nickel is. Both $–NO_2$ and –Cl adsorb strongly on electron-rich nickel, which would result in higher activity in the hydrogenation of the nitro group and dechlorination. In this study, the NiCoB(1:0.1) catalyst has the highest electron density, and therefore it has the highest activity for hydrogenation of the nitro group and dehalogenation reaction. The Co-dopant could weaken the extent of electron donation from the Ni atoms to the aromatic ring in *p*-CAN, which would further suppress the hydrodechlorination of *p*-CAN.

4. Conclusion

A series of nanosized NiCoB amorphous alloy catalysts with various Co contents was prepared by chemically reacting nickel acetate, cobalt acetate, and sodium borohydride in methanolic solution. The Ni/Co ratio affected the concentration of boron bounded to the nickel and cobalt metals, resulting in the change of surface area, amorphous structure, and hydrogenation activities of the catalysts. XRD patterns of the as-prepared samples confirmed the amorphous nature and nanosize range. The peak intensities of XRD patterns decreased with an increase in the cobalt content in NiCoB catalysts. Doping Co in NiB decreased the particle size and increased the stability of the amorphous NiCoB amorphous alloys. Doping Co in NiB increased the boron content, which in turn increased the electron density of Ni. The NiCoB catalysts showed enhanced catalytic activity and thermal stability, being effective for the hydrogenation of *p*-CNB. Among these catalysts, NiCoB(1:0.1) demonstrated the highest activity. Adding small amount of cobalt into NiB not only increased the dispersion of nickel metal and protected the amorphous structure, but also raised the concentration of boron in the catalysts. With an increase in boron concentration, Ni active sites became more highly unsaturated. Although NiCoB(1:0.1) exhibited the highest activity, its selectivity to *p*-CAN was the lowest. High cobalt loading suppressed the hydrogenation activity of *p*-CNB and maintained the high selectivity to *p*-CAN. The Co-dopant could weaken the extent of electron donation from the Ni atoms to the aromatic ring in *p*-CAN, which would further suppress the hydrodechlorination of *p*-CAN. The selectivity to *p*-CAN was also a function of conversion. Both $–NO_2$ and –Cl are electronegative and hence they have the same tendency to be adsorbed on electron-rich metal. Thus, the dehalogenation reaction increased as the reaction proceeded. The results presented here have shown that the NiCoB amorphous alloy catalyst is a promising catalyst for industrial application.

Acknowledgement

This work was supported by the Ministry of Economic Affairs, Taiwan, Republic of China, under contract number 94-EC-17-A-09-S1-022.

References

[1] R. Baltzly, A.R. Phillips, J. Am. Chem. Soc. 68 (1946) 261.
[2] A.A. Strel'tsova, N.D. Zelinskii, Bull. Acad. Sci. U.S.S.R., Div. Chem. Sci. 56 (1943).
[3] P.N. Rylander, M. Kilroy, V. Coven, Engelhard Ind. Tech. Bull. 6 (1965) 11.
[4] W.P. Dunworth, F.F. Nord, J. Am. Chem. Soc. 74 (1952) 1459.
[5] C.F. Winans, J. Am. Chem. Soc. 61 (1939) 3564.
[6] B.O. Pray, F.C. Trager, assigned to Columbia-Southern Chemical, US Patent 2,791,613 (1957).
[7] B. Coq, A. Tijani, F. Figueras, J. Mol. Catal. 71 (1992) 317.
[8] B. Coq, A. Tijani, R. Dutartre, F. Figueras, J. Mol. Catal. 79 (1993) 253.
[9] H. Greenfield, F.S. Dowell, J. Org. Chem. 32 (1967) 3670.
[10] G.C. Bond, D.E. Webster, N. Y. Acad. Sci., Ann. 158 (1969) 540.
[11] J.R. Kosak, N. Y. Acad. Sci., Ann. 172 (1970) 175.
[12] W.W. Yu, H. Liu, J. Mol. Catal. A 243 (2006) 120.
[13] C. Li, Y. Chen, W.J. Wang, Appl. Catal. A 119 (1994) 185.
[14] A. Metcalfe, M.W. Rowden, J. Catal. 22 (1971) 30.
[15] H.C. Yao, P.H. Emmett, J. Am. Chem. Soc. 84 (1962) 1086.
[16] A. Molnar, G.V. Smith, M. Bartok, in: D.D. Eley, H. Pines, P.B. Weisz (Eds.), Advances in Catalysis, vol. 36, Academic Press, New York, 1998, p. 329.
[17] C. Yoon, D.L. Cocke, J. Non-Cryst. Solids 79 (1986) 217.
[18] J.F. Deng, H.Y. Chen, J. Mater. Sci. Lett. 12 (1993) 1508.
[19] H.M. Wang, Z.B. Yu, H.Y. Chen, J. Yang, J.F. Deng, Appl. Catal. A 129 (1995) L143.
[20] A. Ma, W. Lu, E. Min, U.S. Patent 6,051,528 (2000).
[21] G. Seo, H.J. Chang, J. Catal. 67 (1981) 424.
[22] I.H. Liu, C.Y. Chang, S.C. Liu, I.C. Chang, S.M. Shih, Atmos. Environ. 28 (1994) 3409.
[23] C. Li, Y. Chen, W.J. Wang, Appl. Catal. 119 (1994) 185.
[24] J. Shen, Z. Hu, Q. Zhang, L. Zhang, Y. Chen, J. Appl. Phys. 71 (1992) 5217.
[25] S.P. Lee, Y.-W. Chen, Ind. Eng. Chem. Res. 40 (2001) 1495.
[26] A. Baiker, J. Chem, Soc., Faraday Discuss. 87 (1989) 239.
[27] A. Molnar, G.V. Smith, M. Bartok, Adv. Catal. 36 (1989) 329.
[28] J.F. Deng, H. Li, W.J. Wang, Catal. Today 51 (1999) 113.
[29] Y. Chen, Catal. Today 44 (1998) 3.
[30] S. Yoshida, H. Yamashita, T. Funabiki, T. Yonezawa, J. Chem. Soc., Chem. Commun. (1982) 964.
[31] S. Yoshida, H. Yamashita, T. Funabiki, T. Yonezawa, J. Chem. Soc., Faraday Trans. I 80 (1984) 1435.
[32] H. Yamashita, T. Funabiki, S. Yoshida, J. Chem. Soc., Chem. Commun. (1984) 868.
[33] H. Yamashita, M. Yoshikawa, T. Funabiki, S. Yoshida, J. Chem. Soc., Faraday Trans. I 81 (1985) 2485.
[34] J.H. Sinfelt, Acc. Chem. Res. 20 (1987) 134.
[35] N. Toshima, Y. Wang, Langmuir 10 (1994) 4574.
[36] Y. Wang, H. Liu, Polym. Bull. 25 (1991) 139.
[37] J.S. Bradley, E.W. Hill, C. Klein, B. Chaudret, A. Duteil, Chem. Mater. 5 (1993) 254.
[38] H. Liu, G. Mao, S. Meng, J. Mol. Catal. 74 (1992) 275.
[39] N. Toshima, P. Liu, Chem. Lett. (1996) 729.
[40] W. Yu, Y. Wang, H. Liu, W. Zheng, J. Mol. Catal. A 112 (1996) 105.
[41] Y. Nitta, T. Imanaka, S. Teranish, Bull. Chem. Soc. Jpn. 53 (1980) 3154.
[42] B. Shen, S. Wei, K. Fang, J.-F. Deng, Appl. Phys. A 65 (1997) 295.
[43] Y.Z. Chen, B.J. Liaw, S.J. Chiang, Appl. Catal. A 284 (2005) 97.
[44] Z.B. Yu, M.H. Qiao, H.X. Li, J.F. Deng, Appl. Catal. A 163 (1997) 1.
[45] W.L. Dai, M.H. Qiao, J.F. Deng, Appl. Surf. Sci. 120 (1997) 119.

[46] Y.-W. Chen, T.Y. Hsieh, J. Nanopart. Res. 4 (2002) 445.
[47] S.P. Lee, Y.-W. Chen, J. Nanopart. Res. 3 (2001) 133.
[48] Y.C. Liu, Y.-W. Chen, Ind. Eng. Chem. Res. 44 (2006) 4569.
[49] Y.C. Liu, C.Y. Huang, Y.-W. Chen, Ind. Eng. Chem. Res. 45 (2006) 62.
[50] C.Y. Huang, M.S. Thesis, Department of Chemical Engineering, National Central University, 2005.
[51] J. Deng, J. Yang, S. Sheng, H. Chen, J. Catal. 150 (1994) 434.
[52] J. Yang, Doctoral Dissertation, Fudan University, 1993.
[53] A. Lebugle, U. Axelsson, R. Nyholm, N. Martensson, Phys. Scr. 23 (1981) 825.
[54] T. Dickinson, A.F. Povey, P.M.A. Sherwood, J. Chem. Soc., Faraday Trans. I 73 (1977) 332.
[55] K.S. Kim, W.E. Baitinger, J.W. Amy, N. Winograd, J. Electron Spectrosc. Relat. Phenom. 5 (1974) 351.
[56] N.S. McIntyre, M.G. Cook, Anal. Chem. 47 (1975) 2208.
[57] N.N. Hendrickson, J.M. Hollander, W.L. Jolly, Inorg. Chem. 9 (1970) 612.
[58] W.A. Brainard, D.R. Weeler, J. Vac. Sci. Technol. 15 (1978) 1801.
[59] Y. Okamoto, Y. Nitta, T. Imanaka, S. Teranishi, J. Chem. Soc., Faraday Trans. I 75 (1979) 2027.
[60] Y.Z. Chen, K.J. Wu, Appl. Catal. 78 (1991) 185.
[61] C. Hansch, A. Leo, R.W. Taft, Chem. Rev. 91 (1991) 165.
[62] H. Li, Y. Wu, J. Zhang, W. Dai, M. Qiao, Appl. Catal. A 275 (2004) 199.